NJC

Accepted Manuscript

This is an *Accepted Manuscript*, which has been through the Royal Society of Chemistry peer review process and has been accepted for publication.

Accepted Manuscripts are published online shortly after acceptance, before technical editing, formatting and proof reading. Using this free service, authors can make their results available to the community, in citable form, before we publish the edited article. We will replace this *Accepted Manuscript* with the edited and formatted *Advance Article* as soon as it is available.

You can find more information about *Accepted Manuscripts* in the Information for Authors.

Please note that technical editing may introduce minor changes to the text and/or graphics, which may alter content. The journal's standard Terms & Conditions and the Ethical guidelines still apply. In no event shall the Royal Society of Chemistry be held responsible for any errors or omissions in this *Accepted Manuscript* or any consequences arising from the use of any information it contains.

ROYAL SOCIETY OF CHEMISTRY

www.rsc.org/njc

Synthesis of Ni(II) ion imprinted polymer based on macro-mesoporous silica with enhanced dynamic adsorption capacity: Optimization by response surface methodology

Yan Liu[a,*], Fangfang Liu[a], Minjia Meng[a], Zhanchao Liu[b], Liang Ni[a,*], Guoxing Zhong[c]

[a] School of Chemistry and Chemical Engineering, Jiangsu University, Zhenjiang 212013, China

[b] School of Materials Science and Engineering, Jiangsu University of Science and Technology, Zhenjiang 212003, China

[c] School of Environmental and Chemical Engineering, Jiangsu University of Science and Technology, Zhenjiang 212003, China

* Corresponding author. Tel.: +8615751011770.
E-mail address: ly19821212@163.com

Abstract

In this study, Ni(II) ion imprinted polymer (Ni(II)-IIP) based on macroporous–mesoporous silica (MMS) was optimally synthesized using a response surface methodology (RSM) approach for enhanced dynamic adsorption capacity. MMS was prepared *via* dual-templating routes employing liquid crystalline surfactants and polystyrene beads to improve mass transfer and reduce transport limitations. With dynamic adsorption capacity for Ni(II) as the response, the effects of four variables, i.e. amount of S,S'-bis(α,α'-dimethyl-α''-acetic acid)trithiocarbonate (BDAAT), consumption of acrylamide (AM), reaction time and dosage of 2,2′-azobisisobutyronitrile (AIBN), were investigated to solve complex synthesis process. The predicted appropriate preparation conditions were BDAAT dose 0.07 g, AM dose 0.029 g, reaction time 6.3 h, and AIBN dose 4.54 mg, under which Ni(II)-IIP was prepared and used as adsorbent to remove Ni(II), obtaining the maximum dynamic adsorption capacity (12.96 mg/g). The significance of independent variables and their interactions was studied to explain the specific adsorption question. In addition, the resulting Ni(II)-IIP performed without obvious deterioration after five repeated cycles.

Keywords: response surface methodology, macro-mesoporous silica, ion imprinted, synthesis optimization, Ni(II).

.

1. Introductionc

Mesoporous silica materials have been investigated by many researchers from both fundamental and practical viewpoints [1-2]. Unique characteristics based on their pore structure, pore size uniformity, unusual surface topology and large surface area have opened up a new possibility in the research fields of adsorbents [3-4]. Numerous efforts have been attempted to improve the adsorption properties of mesoporous silica from morphology and composition control. By using different strategies, researchers synthesize various kinds of mesoporous silica materials with controllable morphologies, framework compositions, pore structures and pore sizes [5-7]. But it is worth noting that they usually exhibit considerable resistance of diffusion especially in the case of long transportation distance due to pore size limitation [8].

Through the templating approach based on polymer latexes as templates, macroporous materials with pore size ranging from tens of nanometers to several micrometers can be readily synthesized [9-12]. Because of their large interconnected pores, these macroporous materials can provide excellent performance of mass transport and offer easier accessibility for targets, but their surface area is relatively lower which is disadvantageous for efficient adsorption [13-15]. The incorporation of macropores in mesoporous materials can combine the benefits of mesoporous and macroporous structures. In these materials, the macropores act as channels and facilitate the transport of targets that have to be adsorbed in the mesopores [16-18]. The addition of macropores can improve the efficiency of mesoporous materials as they enhance mass transport and reduce diffusion limitations. Although the macroporous–mesoporous materials mentioned above are effective to adsorption, the selectivity of the metal ion from the complex system is not good enough. In order to solve the problem, a method aimed to improve the selectivity of the ion is necessary.

Ion-imprinted polymers (IIPs) derived from molecular imprinted polymers (MIPs) are synthetic recognition materials that display predetermined selectivity towards a chosen template ion [19-20]. Furthermore, surface ion-imprinted polymers (SIIPs) were employed to overcome the drawbacks of IIPs prepared by conventional technique [21]. The main fields of imprinting include separation processes

(chromatography, solid-phase extraction, and membrane separations), artificial antibodies, and sensors recognition elements [22-24]. However, the challenge of designing and synthesizing IIPs can be a daunting prospect to the uninitiated practitioner. During free radical polymerization, there is a complex formation between template and functional monomer, and the matrix is surrounded by complex and cross-linking monomer, yielding a three-dimensional polymer network where template ions are trapped after completion of polymerization [25-26]. The nature of the resulting material and its binding properties are influenced not only by the composition of prepolymerization mixture but also by the experimental conditions employed, such as the variety and dosage of radical initiator used, polymerization temperature, the type and amount of solvent, and so forth. In addition, lots of researches have employed reversible addition-fragmentation chain transfer (RAFT) reagents to synthesize polymers with well-defined structures [27]. That would make it more difficult to synthesize an excellent SIIPs. Based on the above considerations, the optimization of appropriate polymerization conditions are crucial for the improvement of SIIPs performance.

Response surface methodology (RSM) is a collection of statistical and mathematical techniques useful for developing, improving, and optimizing processes in which a response of interest is influenced by several variables and the objective is to optimize this response. It defines the effect of the independent variables, alone or in combination, on the processes [28-30]. Nowadays, it is clearly seen that RSM has been widely applicable in a wide variety of chemical processes, such as the production of microporous palm shell based activated carbon [31], nano-crystalline TiO_2 thin films coated on hollow glass microspheres (HGMs) [32], hydrogel [33], and so on. A critical appraisal of these reported references show how various process variables through RSM could improve the properties of the product. Central composite design (CCD), one type of RSM, is the most commonly used second-order design [34]. It is more efficient and easier to arrange and interpret the optimization experiments compared with other methods.

In this study, we first synthesized macroporous–mesoporous silica (MMS) *via* a

dual-template approach. Then, conduct process optimization using the RSM approach was carried out for the development of Ni(II) ion imprinted polymer (Ni(II)-IIP) based on MMS with enhanced adsorption capacity. There is very little information in the literature using macro-mesoporous silica as the substrate material to synthesize IIPs, and novelty in the present study lies in the use of RSM approach for synthesis process optimization. Different preparation variables on the characteristics of Ni(II)-IIP were studied to find the optimum conditions. In addition, dynamic selectivity and regeneration were also discussed.

2. Experimental

2.1. Materials

Pluronic P123, triblock poly-(ethylene oxide)-poly (propylene oxide)-poly (ethylene oxide), ($EO_{20}PO_{70}EO_{20}$, molecular weight 5800) was purchased from Sigma (USA). Styrene (St), 3-(methacryloxyl) propyltrimethoxysilane (MPS), Ethylene glycol dimethacrylate (EGDMA), Acrylamide (AM) and 2,2′-azobisisobutyronitrile (AIBN) were purchased from the Aladdin Reagent Co., Ltd. (Shanghai, China). Polyvinylpyrrolidone (PVP), tetraethyl orthosilicate (TEOS), and $Ni(NO_3)_2$ were obtained from Sinopharm Chemical Reagents Co. Ltd. (Shanghai, China). The chain transfer agent of S,S'-bis(α,α'-dimethyl-α''-acetic acid)trithiocarbonate (BDAAT) was synthesized according to the reported literatures [35].

2.2. Preparation of Ni(II)-IIP

The dispersion polymerization approach of Sen and coworkers was adopted to generate monodisperse polystyrene (PS) beads [36]. For a typical preparation, 2 g of styrene, 1.6 g of PVP, 0.5 g of MPS and 0.04 g of AIBN were dissolved in a mixture of ethanol (28 mL) and H_2O (2 mL). The obtained solution was then added into a 100 mL three-neck round bottom flask equipped with a mechanical stirrer, a refluxing condenser, and a nitrogen inlet. After sealing in a nitrogen atmosphere, the reactor was submerged in a water bath and polymerization was carried out with a stirring speed of 300 rpm at 70 °C for 24 h. The resulting polymer microspheres were repeatedly washed with an ethanolwater mixture (1:1, v:v) by centrifugation.

Macroporous–mesoporous silicas were synthesized following the approach of Zhao et al. [37], with the addition of polystyrene beads during the synthesis to create macropores. Typically, 2.0 g of P123 was dissolved in 15 mL of water and 50 mL of 2 M HCl solution while stirring at 35 ^{o}C. 1.0 g of polystyrene beads were then added to the solution and stirred for an hour. 4.6 mL of TEOS were added to the solution, which was maintained at 35 ^{o}C for 24 h while stirring. The mixture was then aged at 80 ^{o}C for 24 h and the solid product filtered, washed 3 times with deionised water, and calcined statically in air at 550 ^{o}C (ramp rate of 1 ^{o}C/min) for 6 h. The final solids abbreviated as MMS. A pure mesoporous SBA-15 silica for comparison was also

synthesised for comparison in the absence of polystyrene.

0.3 g of MMS was dispersed in 40 mL of ethanol and the mixture was sonicated for 10 min. Then 2 mL of MPS was added. The reaction was kept at 40 °C for 12 h. The product was separated by centrifuge and washed with ethanol. Finally, the resulting material (MMS@MPS) was dried under vacuum at 50 °C overnight. Using the same method, SBA-15@MPS was prepared by modified SBA-15.

Typically, 0.1 mmol (29.1 mg) of $Ni(NO_3)_2$, an appropriate amount of AM, 1 mmol (0.19 mL) of EGDMA, a know amount of BDAAT, and 50 mg of MMS@MPS were dispersed into a 15.0 mL methanol/distilled water solutions (1:1, v:v). After sealing, shaking, and purging the mixture with nitrogen, a 5.0 mL methanol/distilled water solutions (1:1, v:v) with an appropriate amount of AIBN was added into the suspension. The resultant mixture was stirred at 65 °C for a know time under nitrogen protection. The products extensively washed with methanol/distilled water (1:1, v:v) for several times. Then, the solid was treated with 2 mol/L HCl until no Ni(II) ion was detected in the wash solutions. At last, the polymer was centrifuged with distilled water to neutralization, dried at 50 °C under vacuum. Nonimprinted control polymers (NIP) were synthesized under identical conditions in the absence of Ni(II) ion. For comparison, Ni(II)-IIP-S was prepared in the same manner except using SBA-15 substitute MMS.

2.3. Characterization

VISTA-MPX Inductive Coupled Plasma-Atomic Emission Spectrometer (ICP-AES, Varian, USA) was used to determine the concentrations of Ni(II) and other mental ions. Fourier transmission infrared spectra were separately recorded in a FT-IR spectrophotometer (NEXUS 470 FT-IR apparatus, Nicolet, USA) over the range of 4000–400 cm^{-1}, The crystal phases of the samples were determined by XRD with Cu Ka radiation (model D8 diffractometer, Bruker, Germany). The morphologies of Ni(II)-IIP and support were observed by a scanning electron microscope (SEM, JEOL, JSM-6480) and a transmission electron microscope (TEM, JEOL, JEM-2100). Thermogravimetric analysis (TGA) was carried out using a DSC/DTA-TG (STA 449C Jupiter Netzsch, Germany).

Brunauer−Emmett−Teller (BET) surface area of dried samples was analyzed by nitrogen adsorption in a Micromeritics ASAP 2000 nitrogen adsorption apparatus using the adsorption data in the relative pressure (p/p_0) range of 0.05−0.3. The nitrogen adsorption volume at the relative pressure (p/p_0) of 0.98 was used to determine the pore volume. The desorption isotherm was used to determine the pore size distribution via the Barret−Joyner−Halender (BJH) method. All samples were degassed before nitrogen adsorption measurements.

Porous structures of the samples were analyzed by using a mercury porosimeter (Micromeritics Autopore 9500). In order to perform analysis, samples were weighed and loaded onto a penetrometer which consists of a sample cup integrated with a metal-clad and glass capillary stem, followed by outgassing from sample in a vacuum. Then the penetrometer was automatically filled with mercury. Pore size distribution (PSD) curve was determined from the mercury intrusion data. Under the assumption that all pores are cylindrical, the pore diameter d_p was calculated from the value of p using a well-known capillary law [38]:

$$d_p = \frac{4\gamma \cos\theta}{p} \tag{1}$$

where γ and θ denote the surface tension of mercury and the contact angle of mercury with the sample, respectively.

2.4. Experimental design

Central composite design (CCD) was used to optimize preparation parameters with adsorption capacity of resulting Ni(II)-IIP for Ni(II) as the response. The four significant independent variables considered in this study were dosage of BDAAT (X_1), dosage of AM (X_2), reaction time (X_3), and dosage of AIBN (X_4). CCD was characterized by three operations namely: $2n$ axial runs, 2^n factorial runs and six center runs (n is the number of factors). For this case, it translated to 8 axial points, 16 factorial points and 6 replicates at the center which gives a total of 30 experiments [28].

The usual code of ±1 was used to represent the sixteen factorial points, ±α represented the eight axial points, and the six replicates located at the center (0, 0, 0)

were run. Alpha (α) is the distance of the axial point from center had its value fixed at α=2.0. The coded points and their corresponding values were presented in **Table 1**. (See an example of table presentation in Table 1).

Table 1 Experimental ranges and levels of the independent variables.

Factors	Symbol	Actual values of coded levels				
		-α*	-1	0	1	+α
RAFT dose (g)	X_1	0.01	0.03	0.05	0.07	0.09
AM dose (g)	X_2	0.006	0.017	0.029	0.040	0.052
Reaction time (T)	X_3	2	4	6	8	10
AIBN dose (mg)	X_4	2	4	6	8	10

Note: α = 2.

The response variable was fitted by a second-order model in the form of quadratic polynomial equation:

$$Y = b_0 + \sum_{i=1}^{n} b_{ii} x_i + \sum_{i=1}^{n} b_{ii} x_i^2 + \sum_{i=1}^{n-1} \sum_{j=i+1}^{n} b_{ij} x_i x_j + \varepsilon \qquad (2)$$

where Y is predicted response (predicted adsorption capacity), x_i, x_j are independent variables in coded levels, b_i, b_{ii}, b_{ij} are coefficients for linear, quadratic and interaction effect, respectively, b_0 is model coefficient, n is the number of factors (independent variables), and ε is model error. The quality of fit of polynomial model was expressed by value of correlation coefficient (R^2). The main indicators demonstrating the significance and adequacy of used model include model F-value (Fisher variation ratio), probability value (prob>F), and adequate precision [39].

2.5. Adsorption studies

Fixed-bed adsorption tests were performed using a glass column with 20 cm height and 1 cm internal diameter at 25 °C. A known quantity 0.1 g of Ni(II)-IIP was measured into column to give the desired 0.5 cm bed height. To avoid nonuniform flow (axial dispersion) of the solution and fluidization, some quantity of glass wool were placed in column. Feeding solution with 30 mg/L initial Ni(II) concentration was transported using peristaltic pump from the top of column down to the bottom with flow rate of 1 mL/min. The effluents were collected at a fixed time interval, until the effluent Ni(II) concentration was nearly equal to influent concentration. The

concentration of Ni(II) was tested by ICP-AES.

The breakthrough curves were usually expressed by the plot of C_t/C_0 versus reaction time under various conditions. C_t and C_0 are concentration of metal ions (mg/L) in the effluent and influent, respectively.

For a given flow rate and influent concentration, maximum adsorption capacity of column, q_{total} (mg), is obtained using Eq. (3):

$$q_{total} = \frac{QA_c}{1000} = \frac{Q}{1000}\int_{t=0}^{t=t_{total}} C_{ad}dt \quad (3)$$

where Q is volumetric flow rate (mL/min) and t_{total} is total flow time (min). Meanwhile, equilibrium uptake column capacity (q_{eq}) is derived as the quantity adsorbed (q_{total}) per weight of adsorbent:

$$q_{eq} = \frac{q_{total}}{m} \quad (4)$$

where m is dry weight of adsorbent in column (g).

Batch experiments were carried out to obtain static adsorption capacity. The adsorption capacity Q_e (mg g^{-1}) at equilibrium is calculated as follows:

$$Q_e = \frac{(C_0 - C_e)V}{W} \quad (5)$$

where C_0 (mg L^{-1}) and C_e (mg L^{-1}) are concentrations of Ni(II) at initial and equilibrium, respectively. V (mL) and W (g) are the volume of solution and the mass of adsorbent, respectively.

2.6. Dynamic desorption experiments

An amiable quality of an adsorbent is its predisposition for reuse. This was investigated through desorption and regeneration studies which were valuable attributes in adsorption processes. The dynamic desorption experiment was carried out by using pre-adsorbed Ni(II)-IIP as the sample and 2 M HCl solution as an eluent.

3. Results and discussion

3.1. Preparation of Ni(II)-IIP

The synthesis of Ni(II)-IIP could be simply divided into four steps as follows: (1) Preparation of PS beads. Monodisperse PS beads can be synthesized by dispersion polymerization approach. (2) Preparation of macro-mesoporous silica. In this step, PS beads and P123 were as dual-templating to form macro and mesopores. macroporous–

mesoporous silica combined the benefits of mesoporous and macroporous structures. (3) Surface Modification of MMS. In this step, MPS was reacted with the MMS. The C=C was introduced onto the surface of MMS. (4) Preparation of Ni(II)-IIP. Imprinting was conducted in this step, yielding a three-dimensional polymer network where template Ni(II) was trapped. Then, chelated Ni(II) was eluted by 2 mol/L HCl. Finally, a novel Ni(II)-IIP based on macroporous–mesoporous silica was obtained.

3.2. Characterization

3.2.1. FT-IR spectra

FT-IR spectra of (a) polystyrene; (b) MMS; (c) Ni(II)-IIP were given in **Fig. 1**. For PS (**Fig. 1a**), the band around 3060 cm^{-1} and 3027 cm^{-1} was attributed to aliphatic C-H stretching vibration. The bands at 2924 cm^{-1} and 2846 cm^{-1} were the characteristic adsorption peaks of $-CH_3$ and $-CH_2-$, respectively. The adsorption peaks at 1945, 1872, 1801 and 1601 cm^{-1} assigned to benzene rigid vibration. The sharp band at 540 cm^{-1} corresponded to twist vibration of C=C of vinyl compound. After the calcination, the obtained MMS showed adsorption bands of silica at 1090 cm^{-1}, adsorbed water at 1640 cm^{-1}, and hydroxyl group at around 3500 cm^{-1}, and no band associated with organic species was detected, suggesting the full decomposition of polymer microsphere templates and surfactant templates. These results demonstrated the successful synthesis of macro-/mesoporous silica materials by using the polystyrene and block copolymer P123 as dual templates. Ni(II)-IIP (**Fig. 1c**) exhibited obvious adsorption bands around 1733 cm^{-1}, which was due to the C=O stretching vibration. The adsorption peaks at 1635 and 1458 cm^{-1} assigned to amide I and $–CH_2-$ deformation characteristic adsorption, respectively. These results suggested that Ni(II)-IIP was successfully synthesized. (See an example of artwork presentation in Figure 1).

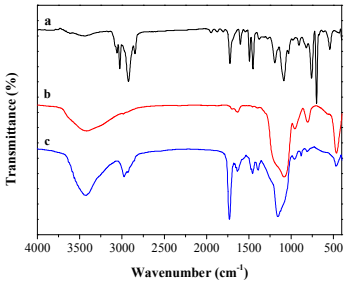

Fig. 1 FT-IR spectra of (a) PS; (b) MMS; (c) Ni(II)-IIP.

3.2.2. Surface morphology

The surface morphology of a) polystyrene, b) SBA-15 and c) MMS were studied by scanning electron microscopy. The as-prepared PS microspheres had a mean diameter of ~1.2 μm with a standard size deviation of less than 5% (**Fig. 2a**). SEM of the undoped SBA-15 revealed a rod-like morphology characteristic of this class of material [40]. The addition of PS beads modified the SBA-15-like organization, creating a new macroporous network. It was interesting to note that the macropores were open and thus well-suited to promote rapid transfer through particle diffusion.

TEM images of the obtained MMS showed macropores of ca. 1.1 μm (**Fig. 3a**). Mesopore character showed that the typical mesoporous structure of SBA-15 was retained in MMS **(Fig. 3b)**. The pore sizes of MMS were observed to be ca. 5-6 nm, with a wall thickness of ca. 6-7 nm. After polymerization, thin polymer layers were formed onto the surface of the MMS **(Fig. 3c)**. The polymer layer had a thickness of about 20 nm and appeared to be uniform, which could be attributable to the intrinsic characteristics of the controlled/living polymerization mechanism of the RAFT polymerization process [41]. (See an example of artwork presentation in Figure 2). (See an example of artwork presentation in Figure 3).

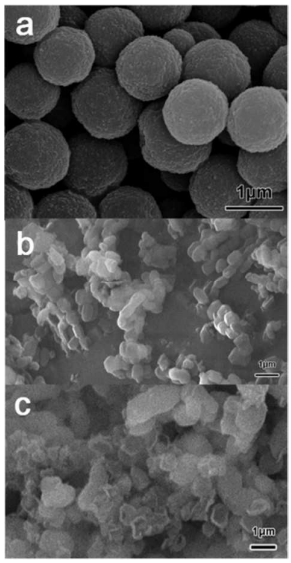

Fig. 2 SEM images of: a) PS beads; b) SBA-15 and c) MMS.

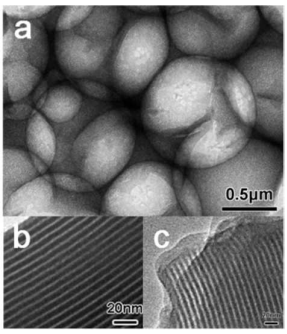

Fig. 3 TEM images of: a) macropore structures in MMS; mesopore structures in b) MMS and c) Ni(II)-IIP.

3.2.3. Characterization of pores

Nitrogen adsorption-desorption isotherms showed all materials exhibit Type IV adsorption isotherms with type-H1 hysteresis loops characteristic of bottlenecked pore openings evident in **Fig. 4A**, which was a characteristic of mesoporous materials. Pure mesoporous SBA-15 had the largest BET specific surface area, pore size and pore volume. Compared with pure SBA-15, the addition of PS beads created new macropores morphology. However, the introduction of macropores didn't affect its mesoporous characteristics, the BET specific surface area, pore size and pore volume of MMS were all similar to SBA-15. After polymerization, the BET specific surface area had a different degree of reduction for different synthesis conditions. **Fig. 4A c-e** were Ni(II)-IIP prepared with a AM loading of 0.006 g, 0.029 g, 0.052 g, respectively

(the samples c, d, and e correspond to entries 13, 6, and 20 in **Table 3**, respectively), which were abbreviated as Ni(II)-IIP-0.006, Ni(II)-IIP-0.029, Ni(II)-IIP-0.052, respectively. The BET specific surface area decreased from 479.4 to 272.5 m^2/g as the amount of AM was increased from pristine MMS to Ni(II)-IIP-0.052. The similar trend was observed for the total pore volume decreasing from 1.194 to 0.815 cm^3/g, concomitant with the narrow pore size distribution ranging from 5.5 to 3.4 nm (Fig. 4B and **Table 2**). These results can be explained that the attachment of polymer layers on the MMS surfaces decreased specific surface area and pore sizes and subsequently limited the diffusion. NIP was synthesized using the same procedure as Ni(II)-IIP-0.029, but in the absence of Ni(II) ion. Comparison of Ni(II)-IIP-0.029 and NIP showed that the BET surface area, pore volume and pore size of the former were slightly larger than those of the latter, probably owing to those cavities left after the elution of Ni(II). (See an example of artwork presentation in Figure 4). (See an example of table presentation in Table 2). (See an example of table presentation in Table 3).

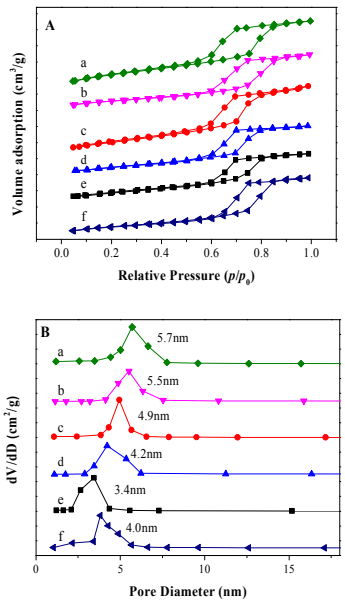

Fig. 4 Nitrogen adsorption–desorption isotherms (A) and pore size distribution (B) of a) SBA-15; b) MMS; Ni(II)-IIP prepared with a AM loading of 0.006 g (c), 0.029 g (d), 0.052 g (e), respectively (the samples c, d, and e correspond to entries 13, 6, and 20 in Table 2, respectively) and (f) NIP.

Table 2 Physical parameters of SBA-15, MMS, Ni(II)-IIP prepared with a AM loading of 0.006 g, 0.029 g, 0.052 g, respectively measured by N_2 adsorption-desorption isotherms and NIP.

Samples	BET surface area	Pore size (nm)	Pore volume (cm^3/g)
SBA-15	490.6	5.7	1.212
MMS	479.4	5.5	1.194
Ni(II)-IIP-0.006	436.0	4.9	1.098
Ni(II)-IIP-0.029	374.7	4.2	1.024
Ni(II)-IIP-0.052	272.5	3.4	0.815
NIP	352.7	4.0	0.975

Table 3 CCD and results for the study of four experimental variables in actual units.

Run	Actual levels				Ni(II) adsorption capacity (mg/g)	
	X_1 (g)	X_2 (g)	X_3 (h)	X_4 (mg)	Experimental	Predicted
1	0.05	0.029	10	6	11.2	10.96
2	0.03	0.040	8	8	10.2	10.16
3	0.07	0.017	4	8	8.2	8.33
4	0.07	0.017	4	4	8.6	8.56
5	0.05	0.029	6	6	12.1	12.32
6	0.05	0.029	6	6	12.3	12.32
7	0.03	0.040	8	4	10.4	10.63
8	0.07	0.040	4	4	12.2	12.35
9	0.05	0.029	2	6	10.4	10.36
10	0.07	0.040	8	4	12.1	12.08

11	0.07	0.017	8	8	9.8	9.96
12	0.05	0.029	6	2	11.4	11.36
13	0.05	0.006	6	6	5	4.79
14	0.07	0.040	4	8	11.2	11.23
15	0.09	0.029	6	6	12.8	12.58
16	0.03	0.040	4	4	11.9	11.66
17	0.03	0.017	8	4	9.2	9.09
18	0.05	0.029	6	6	12.6	12.32
19	0.05	0.029	6	10	10.9	10.66
20	0.05	0.052	6	6	9.3	9.23
21	0.07	0.040	8	8	10.7	10.85
22	0.05	0.029	6	6	12.4	12.32
23	0.01	0.029	6	6	11.5	11.44
24	0.03	0.040	4	8	11.1	11.28
25	0.07	0.017	8	4	10.1	10.28
26	0.03	0.017	8	8	9.3	9.52
27	0.05	0.029	6	6	12.3	12.32
28	0.05	0.029	6	6	12.2	12.32
29	0.03	0.017	4	4	7.9	8.12
30	0.03	0.017	4	8	8.7	8.64

Mercury penetration was also used to characterize the pores, and the data were shown in **Fig. 5**. The mesopore size distribution of MMS was centered at 5.5 nm, which was consistent with the above nitrogen adsorption-desorption data. And another important data were the second peak of MMS with an average diameter of 1096 nm, the macropores were close to the parent PS beads dimensions. This contrasted with previous reports [42]. Herein notable macropore shrinkage was observed after calcination. After polymerization reaction, the mesopores and macropores of Ni(II)-IIP were reduced to 4.2 nm and 988 nm, respectively. Although there was a slight decrease of macropores, but it can still act as channels and reduce mass transfer

resistance. (See an example of artwork presentation in Figure 5).

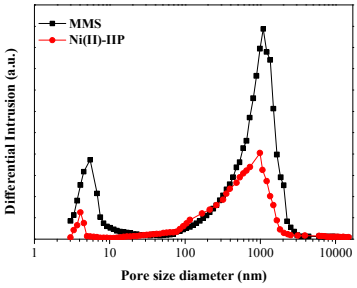

Fig. 5 Pore size distribution determined by mercury porosimetry.

3.2.4. XRD characterization

XRD patterns of MMS and Ni(II)-IIP were presented in **Fig. 6**. All the samples exhibited well defined peaks at 1.01 ^{o}, 1.70 ^{o} and 1.96^{o}, associated with the (100), (110) and (200) planes of the P6mm space group for the hexagonal arrangement of mesoporous channels, suggesting that pore structure is retained after polymerization. However, there is a slight shift of the small-angle shift to higher angles, indicating the decrease in d-spacing [43]. (See an example of artwork presentation in Figure 6).

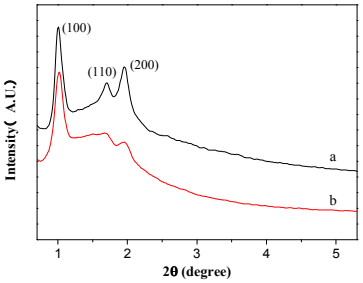

Fig. 6 Low angle powder XRD patterns of: a) MMS; and b) Ni(II)-IIP.

3.2.5. Characteristic of TGA

The thermal behavior of polymers was evaluated by TGA (**Fig. 7**). The first mass loss steps, from about 25 to 100 ^{o}C, were due to the loss of physically adsorbed water on surface of MMS. The high rate of weight loss in temperature ranging from 200 to 800 ^{o}C may be due to the loss of polymer layer. Throughout the analysis, total mass loss of MMS and Ni(II)-IIP were calculated to be 4.78% and 27.16%, respectively. The remaining mass was attributed to the more thermally resistant silicon-based material. (See an example of artwork presentation in Figure 7).

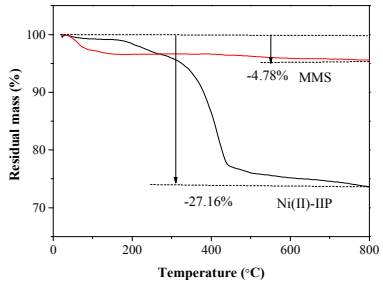

Fig. 7 TGA profiles of MMS and Ni(II)-IIP.

3.3. Discussion of regression model

Table 3 represents the experimental planning matrix with the response variables obtained experimentally. The following equation is a regression model with experimental results:

$$Q_e = +12.32 + 0.28X_1 + 1.11X_2 + 0.15X_3 - 0.18X_4 + 0.063X_1X_2 + 0.19X_1X_3 - 0.19X_1X_4 - 0.50X_2X_3 - 0.22X_2X_4 - 0.025X_3X_4 - 0.077X_1^2 - 1.33X_2^2 - 0.41X_3^2 - 0.33X_4^2 \quad (6)$$

where Q_e is predicted adsorption capacity of Ni(II); X_1, X_2, X_3 and X_4 are coded values of amount of BDAAT, consumption of AM, reaction time and dosage of AIBN, respectively.

Analysis of variance (ANOVA) was used for further justification of the adequacy of model. The significance of each model was assessed from adjusted determination coefficient (R^2_{adj}) which was found to be 0.9838, implying that only 1.62% of variation in Q_e response cannot be explained by this model. The *F*-value for a model was the test for comparing variance associated with that term with residual variance. As it can be seen in **Table 4**, model *F*-value of 127.19 implied that the model was significant. There was only a 0.01% chance that a "Model *F*-value" this large could occur due to noise. The significance of each term in this model was also evaluated by *p*-value (prob>*F*). The smaller *p*-values, the bigger the significance of corresponding variable. *p*-values in this study less than 0.05 indicate model terms were significant. In this case X_1, X_2, X_3, X_4, X_1X_3, X_1X_4, X_2X_3, X_2X_4, X_2^2, X_3^2, X_4^2 were significant model terms. The coefficient of variation (CV) indicated the degree of precision with which the treatments are compared. A lower CV meant a higher reliability of the experiment.

The lower value of CV (2.11%) demonstrated the performed experiments were highly reliable. The value of 0.2233 for "Lack of Fit *F*-value" implied that Lack of Fit was not significant relative to pure error. Non-significant lack of fit was good and showed that the above model was appropriate to predict the adsorption capacity of Ni(II) within the range of variables studied. (See an example of table presentation in Table 4).

Table 4 Analysis of variance for the response of the adsorption capacity for Ni(II).

Sources of variation	Sum of squares	Degree of freedom	Mean square	*F* value	Probability>*F*	Comment
Model	89.43	14	6.39	127.19	< 0.0001	significant
X_1	1.93	1	1.93	38.36	< 0.0001	significant
X_2	29.48	1	29.48	587.02	< 0.0001	significant
X_3	0.54	1	0.54	10.75	0.0051	significant
X_4	0.74	1	0.74	14.63	0.0017	significant
X_1X_2	0.06	1	0.06	1.24	0.2822	
X_1X_3	0.56	1	0.56	11.20	0.0044	significant
X_1X_4	0.56	1	0.56	11.20	0.0044	significant
X_2X_3	4.00	1	4.00	79.65	< 0.0001	significant
X_2X_4	0.81	1	0.81	16.13	0.0011	significant
X_3X_4	0.01	1	0.01	0.20	0.6618	
X_1^2	0.16	1	0.16	3.25	0.0918	
X_2^2	48.31	1	48.31	961.84	< 0.0001	significant
X_3^2	4.71	1	4.71	93.87	< 0.0001	significant

X_4^2	2.93	1	2.93	58.43	< 0.0001	significant
Residual	0.75	15	0.05			
Lack of fit	0.60	10	0.06	2.04	0.2233	not significant
Pure error	0.15	5	0.03			
Total	90.18	29				

Fig. 8 showed predicted values versus experimental values for Ni(II) adsorption capacity. The obtained experimental values were quite close to predicted values, indicating that the developed model was successful in capturing the correlation between Ni(II)-IIP preparation variables to Ni(II) adsorption capacity. (See an example of artwork presentation in Figure 8).

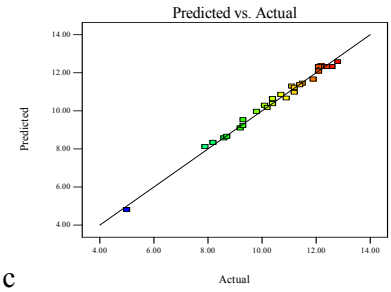

c

Fig. 8 Predicted vs. experimental Ni(II) adsorption capacity of Ni(II)-IIP.

3.4. Effects of process parameters on optimization

Response surface plots and contour plots were shown in **Figs. 9-10**, which provided a method to visualize the relationship between response and experimental levels of each variable and the type of interactions between two test variables. The shapes of the contour plots, circular or elliptical, indicated whether the mutual interactions between variables were significant or not.

The combined effect of amounts of BDAAT (X_1) and AM (X_2) on Ni(II) dynamic adsorption was shown in **Figs. 9a-b**. Obviously, the amount of AM played an important role in controlling final adsorption capacity for Ni(II) during preparation process. It was observed that when the amount of AM was lower than 0.029 g (4 times molecular weight of template ion), adsorption capacity of Ni(II) on Ni(II)-IIP

increased with increasing AM content due to the increase in the number of recognition sites. However, a slight decrease in the adsorption amount could be obtained as the content of AM was above 0.029 g. This was because excessive functional monomers would occur self-polymerization, which made the decrease of recognition sites and specific surface area [44]. Meanwhile, adsorption capacity of Ni(II) increased with increasing BDAAT content. BDAAT, a reversible chain transfer agent, can easily introduce functional groups into the chain ends of polymers and control the chains of polymers with appropriate molar mass and low polydispersity. The more dosage of BDAAT, the more structured polymer layer and higher adsorption capacity. A maximum Ni(II) adsorption (>12 mg/g) was determined at constant T (6 h) and AIBN dose (6 mg).

The interaction relationships of BDAAT (X_1) with reaction time (X_3) on dynamic adsorption of Ni(II) were shown in **Figs. 9c-d**. It was evident that at high value, about >0.045 g, the positive influence of reaction time on Ni(II) adsorption was significant. While in case of the BDAAT dose being below 0.045 g, adsorption capacity of Ni(II) would fall below 12.2 mg/g no matter reaction time was. And for a definite amount of BDAAT, an optimum reaction time existed around 6.3 h. Reaction time was an important condition for synthesis process of imprinted polymers. If reaction time was short, imprinted sites would be relatively poor. Whereas, molecular weight of polymer will be great in the case a long time, causing the polymer layer too thick. A maximum Ni(II) adsorption (>12.4 mg/g) was observed at constant AM dosage (0.029 g) and AIBN dose (6 mg).

In **Figs. 9e-f**, response curve and isogram were drawn as a function of BDAAT (X_1) and AIBN (X_4) doses. It was observed that adsorption capacity increased with increase in BDAAT and AIBN dose. However, up to a certain limit adsorption capacity was decreased by increasing AIBN dose. AIBN was the most common kind of azo initiators. The higher initiator agent content, the higher concentration of active centers, so that polymerization rate was accelerated, thereby affecting the molecular weight of polymer. Thus, the impact of the amount of initiator and reaction time on adsorption capacity had a similar effect. Meanwhile, with the increase of BDAAT, the

amount of AIBN had more and more impact on adsorption capacity. It can be seen that RAFT agent played an important role in reaction. A maximum Ni(II) adsorption (>12.6 mg/g) was observed at constant AM dosage (0.029 g) and T (6 h). (See an example of artwork presentation in Figure 9). (See an example of artwork presentation in Figure 10).

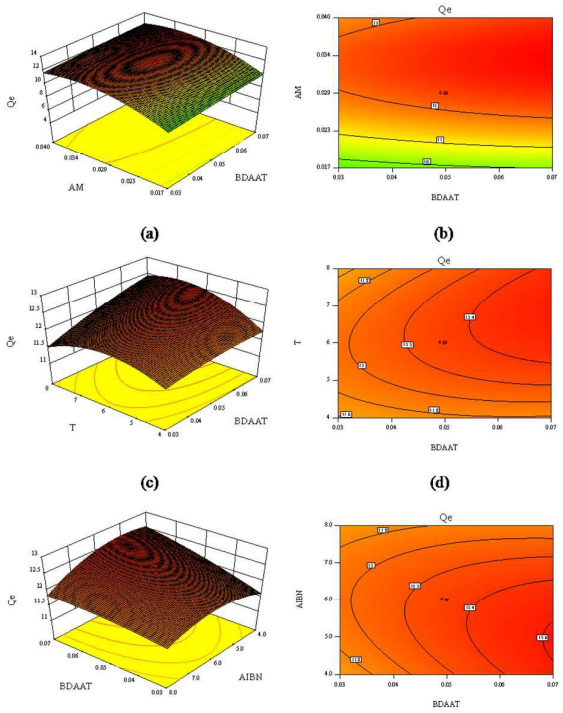

c

Fig. 9 (a) Three-dimensional response surface plot and (b) contour plot of interactions of variables BDAAT and AM doses and its effect on Ni(II) adsorption. (c) Three-dimensional response surface plot and (d) contour plot of interactions of variables BDAAT dose and reaction time and its effect on Ni(II) adsorption. (e) Three-dimensional response surface plot and (f) contour plot of interactions of variables BDAAT and AIBN doses and its effect on Ni(II) adsorption.

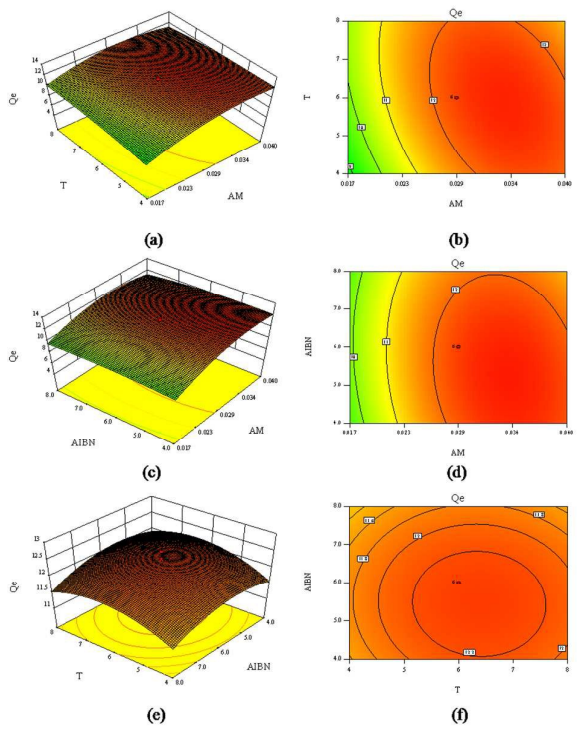

Fig. 10 (a) Three-dimensional response surface plot and (b) contour plot of interactions of variables AM dose and reaction time and its effect on Ni(II) adsorption. (c) Three-dimensional response surface plot and (d) contour plot of interactions of variables AM and AIBN doses and its effect on Ni(II) adsorption. (e) Three-dimensional response surface plot and (f) contour plot of interactions effect of AIBN dose and reaction time and its effect on Ni(II) adsorption.

The effect of AM dose (X_2) and reaction time (X_3) on Ni(II) dynamic adsorption capacity was illustrated in **Figs. 10a-b**. When AM dose and reaction time increased simultaneously, adsorption capacity increased and then decreased. This can be explained by the above conclusion. The binding sites were increasing rapidly when both were increased. But when AM dose and reaction time were extreme, self-polymerization and excessive growth of chain occurred simultaneously, causing the decrease of binding sites and specific surface area. A maximum Ni(II) adsorption (>12 mg/g) was observed at constant BDAAT dosage (0.05 g) and AIBN dose (6 mg).

Figs. 10c-d gave a clear idea about the effect of AM (X_2) and AIBN (X_4) doses on Ni(II) dynamic adsorption. It can be seen that **Fig. 10d** and **Fig. 10b** showed

similar pattern. Therefore, the above theory can also be used to explain these trends. A maximum Ni(II) adsorption (>12 mg/g) was observed at constant BDAAT dosage (0.05 g) and T (6 h).

The effect of reaction time (X_3) and AIBN dose (X_4) on Ni(II) dynamic adsorption capacity was illustrated in **Figs. 10e-f**. It can be concluded that Ni(II) adsorption capacity increased with reaction time within 5.1-7.6 h range and AIBN dose within 4.1-6.8 mg range. At constant BDAAT (0.05 g) and AM (0.029 g) dose, a maximum Ni(II) removal of >12.2 mg/g was determined.

3.5. Validation of models

To confirm the goodness of the model for predicting maximal Ni(II) adsorption capacity, additional experiments in triplicate using these optimized conditions were carried out. According to the results of statistical design, the optimized preparation conditions were as follows: BDAAT dose 0.07 g, AM dose 0.029 g, reaction time 6.3 h, and AIBN dose 4.54 mg, obtaining maximum dynamic adsorption capacity (12.96 mg/g) of Ni(II). To ensure the predicted result was not bias the practical value, experiment rechecking was performed using modified optimal conditions: BDAAT dose 0.07 g, AM dose 0.029 g, reaction time 6.3 h, and AIBN dose 4.5 mg. A mean value of 12.83 ± 0.23 mg/g (N=3) was gained, which was in agreement with the predicted value significantly, demonstrated the validation of RSM model.

3.6. Comparison of different adsorbents

In order to verify the superiority of macro-mesoporous silica, dynamic adsorption properties of Ni(II)-IIP, Ni(II)-IIP-S and NIP were studied. The results were shown in **Fig. 11**. Compared with Ni(II)-IIP-S, Ni(II)-IIP exhibited higher dynamic adsorption capacity. The adsorption capacity of Ni(II)-IIP was 12.16 mg/g, more than that of Ni(II)-IIP-S (7.59 mg/g). The results proved that the introduction of macropores may act as channels and facilitate the transport of Ni(II) to be adsorbed in mesopores, thus favoring mass transfer and reducing transport limitations. And the adsorption capacity of Ni(II)-IIP was also much higher than NIP, this result proved excellent adsorption ability of Ni(II)-IIP due to the specific binding sites. (See an example of artwork presentation in Figure 11).

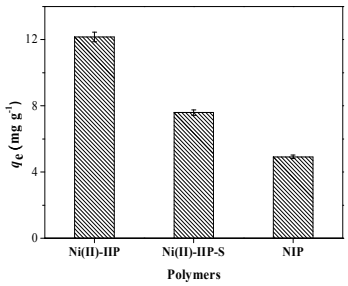

Fig. 11 Adsorption study of different adsorbents.

Nowadays, there was few literatures investigating the dynamic adsorption on Ni(II). In this study, dynamic adsorption is the main adsorption mode. But the fact that the adsorption capacity of dynamic mode was much smaller than that of static has been proved in lots of literatures [45]. Hence, Static adsorption studies were also carried out to research the property of Ni(II)-IIP. A comparison of the maximum static capacity (Q_{max}) of Ni(II) onto Ni(II)-IIP with those of other adsorbents reported in the literatures is given in **Table 5**. It was obviously seen that Ni(II)-IIP had the highest adsorption capacity (92.48 mg g^{-1}) among these adsorbents. (See an example of table presentation in Table 5).

Table 5 Comparison of maximum adsorption of Ni(II) ions onto various adsorbents.

Sorbent	Maximum adsorption capacity (mg/g)	Reference
Cashew nut shell	18.87	[46]
ECH crosslinked chitosan–clay beads	32.36	[47]
Fe3O4–TW	38.30	[48]
IIP	40.26	[49]
RAFT-IIP	81.73	[50]
Ni(II)-IIP	92.48	This study

3.7. Competitive adsorption of Ni(II)-IIP

The effect of interference of coexisting ions of Cd(II), Co(II),Cu(II) and Zn(II) (30 mg/L) with Ni(II) ion (30 mg/L) on the adsorption of Ni(II) was studied using the dynamic procedure. Adsorption capacities of the Ni(II)-IIP and NIP for metal ions under competitive conditions were given in **Fig. 12**. Ni(II)-IIP exhibited good

adsorption selectivity for Ni(II) in the presence of competitive metal ions. And it was obviously that adsorption capacity of Ni(II)-IIP was higher than that of NIP, which were due to the presence of specific cavities on imprinted adsorbents. (See an example of artwork presentation in Figure 12).

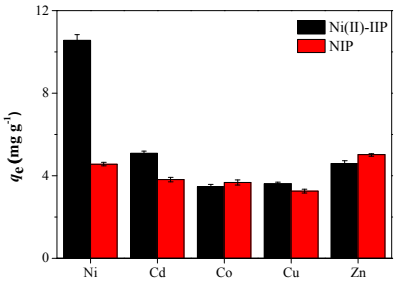

Fig. 12 Competitive adsorption of Ni(II) and metal ions on Ni(II)-IIP and NIP.

3.8. Reusability of Ni(II)-IIP

For economic reasons, the recyclability of spent adsorbent is a key evaluation factor. Several eluents were tried in order to regenerate Ni(II)-IIP. The desorption of Ni(II) is 87.6%, 92.1%, and 97.8% for 2.0 mol/L HNO_3, 2.0 mol/L H_2SO_4, and 2.0 mol/L HCl, respectively. Among them 2.0 mol/L HCl was proved to be a relatively effective eluent for desorption of Ni(II) ions from Ni(II)-IIP. Adsorption-desorption results of repeated uses in Ni(II)-IIP were shown in **Fig. 13**. It is stable for up to five adsorption cycles without obvious decrease in the removal efficiency for Ni(II). The experimental results indicate that Ni(II)-IIP had excellent regeneration ability. (See an example of artwork presentation in Figure 13).

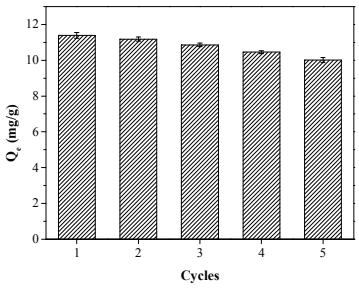

Fig. 13 Stability and potential regeneration of Ni(II)-IIP.

4. Conclusion

Response surface methodology was applied for optimizing the preparation parameters to obtain Ni(II) ion imprinted polymer with excellent adsorption properties for Ni(II). The use of macro-mesoporous silica matrix significantly improved the adsorption capacity of imprinted polymer. The statistical analysis results showed that the appropriate preparation conditions were as follows: S,S'-bis(α,α'-dimethyl-α''-acetic acid)trithiocarbonate dose 0.07 g, acrylamide dose 0.029 g, reaction time 6.3 h, and 2,2′-azobisisobutyronitrile dose 4.54 mg. Among four parameters, the amount of acrylamide was the most important one in controlling the final adsorption capacity. Moreover, the prepared Ni(II) ion imprinted polymer exhibited a good selectivity of Ni(II) and eluting performance.

Acknowledgments

This work was financially supported by the National Natural Science Foundation of China (Nos. 21207051), Ph.D. Programs Foundation of Ministry of Education of China (No. 20123227120015), Natural Science Foundation of Jiangsu Province (BK20150483), China Postdoctoral Science Foundation funded project (No. 2012M511220), Special Financial Grant from the China Postdoctoral Science Foundation (2014T70488), Natural science fund for Colleges and Universities in Jiangsu Province (No. 15KJB550003), Society Development Fund of Zhenjiang (Nos. SH2012021, SH2013110), Programsof Senior Talent Foundation of Jiangsu University (No. 15JDG024)

[1] Z. A. ALOthman, *Mater.*, 2012, **5**, 2874-2902.

[2] Y. Wan and D. Zhao, *Chem. Rev.*, 2007, **107**, 2821-2860.

[3] J. R. Deka, C. L. Liu, T. H. Wang, W. C. Chang and H. M. Kao, *J. Hazard. Mater.*, 2014, **278**, 539-550.

[4] S. Egodawatte, A. Datt, E. A. Burns and S. C. Larsen, *Langmuir*, 2015, **31**, 7553-7562.

[5] A. Salis, D. Meloni, S. Ligas, M. F. Casula, M. Monduzzi, V. Solinas and E. Dumitriu, *Langmuir*, 2005, **21**, 5511-5516.

[6] S. Huh, J. W. Wiench, J. C. Yoo, M. Pruski and V. S. Y. Lin, *Chem. Mater.*, 2003, **15**, 4247-4256.

[7] T. W. Kim, F. Kleitz, B. Paul and R. Ryoo, *J. Am. Chem. Soc.*, 2005, **127**, 7601-7610.

[8] G. Ma, X. Yan, Y. Li, L. Xiao, Z. Huang, Y. Lu and J. Fan, *J. Am. Chem. Soc.*, 2010, **132**, 9596-9597.

[9] Z. Wang, E. R. Kiesel and A. Stein, *J. Mater. Chem.*, 2008, **18**, 2194-2200.

[10] C. Xue, J. Wang, B. Tu and D. Zhao, *Chem. Mater.*, 2009, **22**, 494-503.

[11] M. Wang, X. Wang, Q. Yue, Y. Zhang, C. Wang, J. Chen, H. Cai, H. Lu, A. A. Elzatahry, D. Zhao and Y. Dencg, *Chem. Mater.*, 2014, **26**, 3316-3321.

[12] Y. Deng, C. Liu, T. Yu, F. Liu, F. Zhang, Y. Wan, L. Zhang, C. Wang, B. Tu, P. A. Webley, H. Wang and D. Zhao, *Chem. Mater.*, 2007, **19**, 3271-3277.

[13] F. Q. Liu, L. Wang, Z. G. Huang, C. Q. Li, W. Li, R. X. Li and W. H. Li, *ACS Appl. Mater. Inter.*, 2014, **6**, 4371-4381.

[14] A. Walcarius, *TrAC Trends Anal. Chem.*, 2012, **38**, 79-97.

[15] Z. Sun, Y. Deng, J. Wei, D. Gu, B. Tu and D. Zhao, *Chem. Mater.*, 2011, **23**, 2176-2184.

[16] T. Kamegawa, S. Tanaka, H. Seto, D. Zhou and H. Yamashita, *Phys. Chem. Chem. Phys.*, 2013, **15**, 13323-13328.

[17] R. Ravetti-Duran, J. L. Blin, M. J. Stébé, C. Castel and A. Pasc, *J. Mater. Chem.*, 2012, **22**, 21540-21548.

[18] M. Wang, Z. Sun, Q. Yue, J. Yang, X. Wang, Y. Deng, C. Yu and D. Zhao, *J. Am.*

Chem. Soc., 2014, **136**, 1884-1892.

[19] C. Branger, W. Meouche, A. Margaillan, *React. Funct. Polym.*, 2013, **73**, 859-875.

[20] G. Bayramoglu and M. Y. Arica, *J. Hazard. Mater.*, 2011, **187**, 213-221.

[21] H. T. Fan, X. Fan, J. Li, M. Guo, D. Zhang, F. Yan and T. Sun, *Ind. Eng. Chem. Res.*, 2012, **51**, 5216-5223.

[22] E. Najafi, F. Aboufazeli, H. R. L. Z. Zhad, O. Sadeghi and V. Amani, *Food Chem.*, 2013, **141**, 4040-4045.

[23] L. Chen, S. Xu and J. Li, *Chem. Soc. Rev.*, 2011, **40**, 2922-2942.

[24] A. Bahrami, A. Besharati-Seidani, A. Abbaspour and M. Shamsipur, *Electrochim. Acta*, 2014, **118**, 92-99.

[25] P. A. G. Cormack and A. Z. Elorza, *J. Chromatogr. B*, 2004, **804**, 173-182.

[26] J. E. Lofgreen and G. A. Ozin, *Chem. Soc. Rev.*, 2014, **43**, 911-933.

[27] G. Pan, Y. Zhang, X. Guo, C. Li and H. Zhang, *Biosens. Bioelectron.*, 2010, **26**, 976-982.

[28] D. Baş and I. H. Boyacı, *J. Food Eng.*, 2007, **78**, 836-845.

[29] M. A. Bezerra, R. E. Santelli, E. P. Oliveira, L. S. Villar and L. A. Escaleira, *Talanta*, 2008, **76**, 965-977.

[30] T. Ölmez, *J. Hazard. Mater.*, 2009, **162**, 1371-1378.

[31] A. Arami-Niya, W. M. A. W. Daud, F. S. Mjalli, F. Abnisa and M. S. Shafeeyan, *Chem. Eng. Res. Des.*, 2012, **90**, 776-784.

[32] L. Sun, S. Wan, Z. Yu and L. Wang, *Sep. Purif. Technol.*, 2014, **125**, 156-162.

[33] Y. Zheng, Y. Liu and A. Wang, *Chem. Eng. J.*, 2011, **171**, 1201-1208.

[34] S. Mohana, S. Shrivastava, J. Divecha and D. Madamwar, *Bioresour. Technol.*, 2008, **99**, 562-569.

[35] J. T. Lai, D. Filla and R. Shea, *Macromol.*, 2002, **35**, 6754-6756.

[36] T. Sen, G. J. T. Tiddy, J. L. Casci and M. W. Anderson, *Chem. Mater.*, 2004, **16**, 2044-2054.

[37] D. Y. Zhao, J. L. Feng, Q. S. Huo, N. Melosh, G. H. Fredrikson, B. F. Chmelka and G. D. Stucky, *Science*, 1998, **279**, 548–552.

[38] E. W. Washburn, *Proc. Nat. Acad. Sci. USA*, 1921, 115-116.

[39] P. D. Patil, V. G. Gude, A. Mannarswamy, P. Cooke, S. Munson-McGee, N. Nirmalakhandan and S. Deng, *Bioresour. Technol.*, 2011, **102**, 1399-1405.

[40] A. Shahbazi, H. Younesi and A. Badiei, *Chem. Eng. J.*, 2011, **168**, 505–518.

[41] X. Luo, Y. Zhan, Y. Huang, L.Yang, X. Tu and S. Luo, *J. Hazard. Mater.*, 2011, **187**, 274-282.

[42] T. Amatani, K. Nakanishi, K. Hirao and T. Kodaira, *Chem. Mater.*, 2005, **17**, 2114-2119.

[43] S. K. Das, M. K. Bhunia, D. Chakraborty, A. R. Khuda-Bukhsh and A. Bhaumik, *Chem. Commun.*, 2012, **48**, 2891-2893.

[44] S. Xu, J. Li and L. Chen, *J. Mater. Chem.*, 2011, **21**, 4346-4351.

[45] J. M. Arsuaga, J. Aguado, A. Arencibia and M. S. López-Gutiérrez, *Adsorpt.*, 2014, **20**, 311-319.

[46] P. S. Kumar, S. Ramalingam, S. D. Kirupha, A. Murugesan, T. Vidhyadevi and S. Sivanesan, *Chem. Eng. J.*, 2011, **167**, 122–31.

[47] V. N. Tirtom, A. Dinçer, S. Becerik, T. Aydemir and A. Çelik, *Chem. Eng. J.*, 2012, **197**, 379-386.

[48] P. Panneerselvam, N. Morad and K. A. Tan, *J. Hazard. Mater.*, 2011, **186**, 160-168.

[49] S. Abbasi, M. Roushani, H. Khani, R. Sahraei and G. Mansouri, *Spectrochim. Acta Part A*, 2015, **140**, 534-543.

[50] Y. Liu, X. Meng, Z. Liu, M. Meng, F. Jiang, M. Luo, L. Ni, J. Qiu, F. Liu and G. Zhong, *Langmuir*, 2015, **31**, 8841-8851.